Electronic Supplementary Material (ESI) for Nanoscale.

Supporting Information

In-depth atomic force microscopy investigation of nanoscale mechanical properties of Pāua nacre

Cam-Phu Thi Nguyen,[a] Peggy Schoenherr,*[ab] Lyman Juli[a] and Jan Seidel*[ab]

[a]*School of Materials Science and Engineering, UNSW Sydney, Sydney 2052, Australia*

[b]*ARC Centre of Excellence in Future Low-Energy Electronics Technologies (FLEET), UNSW Sydney, Sydney, NSW 2052, Australia*

1. Contact resonance force microscopy method for nanomechanical measurements

Contact resonance force microscopy (CRFM) measures the mechanical properties of a sample by tracking the contact resonance frequency change using the dual AC resonance tracking (DART) mode[1]. As D.C. Hurley *et al.* reported[1-3], the system is either mechanically excited by shaking the cantilever or vibrating the sample using an actuator. During the scanning process, the force between tip and sample is kept constant and the change of contact resonance frequency is tracked. A shift in resonance frequency corresponds to a change of contact stiffness (elastic modulus) of the sample. A stiffer sample area exhibits a shift to higher resonance frequencies while a softer sample shifts to lower values. In this method, the tip and sample are in contact, as shown in Fig. S1. A more extensive discussion on CRFM can be found elsewhere[1–4].

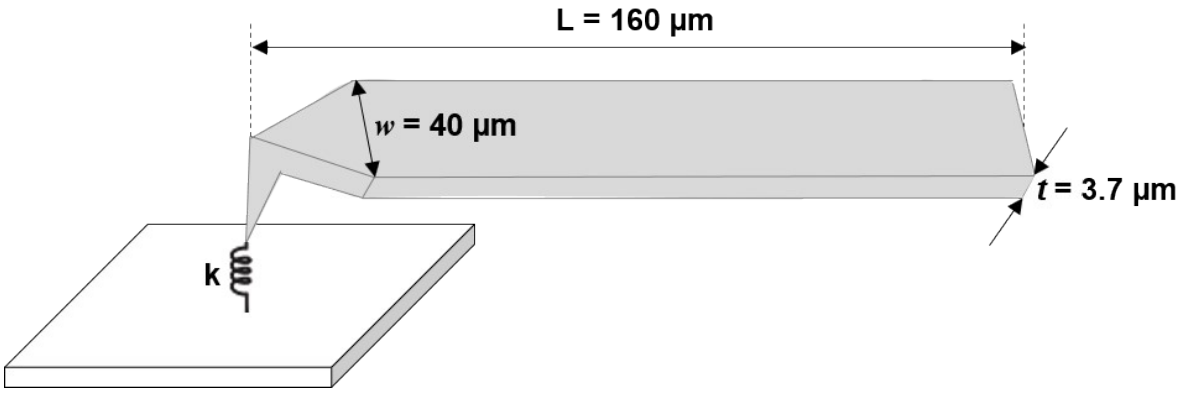

Figure S1. Important tip parameters for the determination of the elastic modulus with spring constant k_{lever}, length L of the cantilever, and tip position ratio γ.

Here, we want to describe the extraction of the elastic modulus from CRFM measurements via the method by D. C. Hurley *et al.*[5]. The AFM cantilever spring constant k_{lever} is connected to the length L, the distance from the end of the cantilever to the tip L_1, the width w, the thickness t, and the elastic modulus E_i by:

$$k_{lever} = \frac{E_i t^3 w}{4L_1^3} \tag{S1}$$

See Fig. S1 for the cantilever parameters. The tip-sample interaction is defined by a contact stiffness with the spring constant k. The normalized contact stiffness k/k_{lever} is given by:

$$\frac{k}{k_{lever}} = \frac{2}{3}(x_n L\gamma)^3 \frac{1+\cos x_n L \cosh x_n L}{D} \tag{S2}$$

where x_n is the wavenumber of the contact resonance frequency f_n; γ is the tip position ratio describing the relationship of L and L_1 as $\gamma = \frac{L_1}{L}$ and D is given by:

$$\begin{aligned} D = &[\sin x_n L(1-\gamma)\cosh x_n L(1-\gamma) - \cos x_n L\gamma \sinh x_n L\gamma][1-\cos x_n L\gamma \cosh x_n L\gamma] \\ &-[\sin x_n L\gamma \cosh x_n L\gamma - \cos x_n L\gamma \sinh x_n L\gamma][1+\cos x_n L(1-\gamma)\cosh x_n L(1-\gamma)] \end{aligned} \tag{S3}$$

The elastic properties of the sample can be determined using the Hertzian model. The contact stiffness k between the tip and sample is given by:

$$k = 2aE_r \tag{S4}$$

with the contact radius a:

$$a = \sqrt[3]{\frac{3RF_N}{4E_r}} \tag{S5}$$

where F_N is the applied load to the tip, R is the tip radius. The relationship between reduced elastic modulus E_r and the sample elastic modulus E is represented as:

$$\frac{1}{E_r} = \frac{1-\nu^2}{E} + \frac{1-\nu_i^2}{E_i} \tag{S6}$$

where ν and ν_i are the Poisson ratio of the sample and the tip, respectively. The elastic modulus values E in the main text can then be calculated by using equation S1-S6 and the cantilever specifications as well as Poisson ratios of the aragonite and biopolymer (all values are presented in Table S1). The spring constant of the tip is determined via the thermal method in the MFP-3D Infinity system (Asylum Research, USA).

Table S1. Tip specifications and sample Poisson ratio values that used in this study

Parameters		Value	Reference
Uncoated tip AC160TSA-R3 (Asylum Research, USA)	Spring constant k_{lever} (N/m)	33	6
	Tip radius R (nm)	7	
	Poisson ratio v_i	0.17	
Sample poisson ratio v	Aragonite	0.16	7
	Biopolymer	0.4	

2. Force-distance curve – Hertzian model

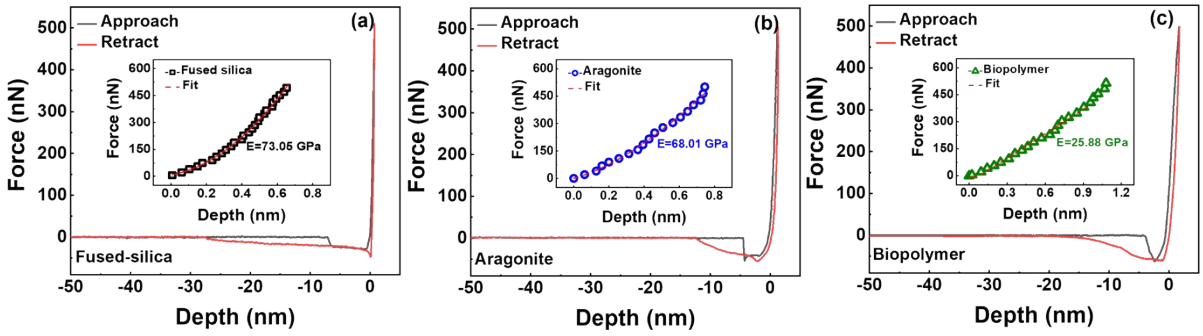

Figure S2. Force-distance curves of (a) standard fused silica, (b) aragonite, and (c) biopolymer areas. The zoom-in to the fitted regions by the Hertzian model to determine the elastic modulus.

Figure S2 (a) represents the force-distance measurements of fused silica (Bruker, USA) using a diamond tip (NM-RC-C, Bruker USA) with force constant k = 470 N/m. The elastic modulus was obtained by fitting the force-distance curve using the Hertzian model, which is embedded in the Asylum software. To determine accurate elastic modulus values the identification of the contact point is crucial[8–10]. The Asylum software defines the contact point when the Set Point deflection voltage is equal to the cantilever Set Point deflection value. This is the point when the cantilever starts to experience positive deflection due to the applied force

from the piezo. This approach has led to good results for AFM-based force-distance curves[8,11]. Using the Asylum software to fit the fused silica force-distance curves results in an elastic modulus value of 73.05 GPa. This is in good agreement with the manufacturer values of fused silica (nominal elastic modulus of 72.9 GPa[12]) and thus, the same cantilever values can be used for all force-distance curves. An example of the biopolymer and aragonite area is shown in Fig. S2(b) with a representative elastic modulus of 25.88 GPa for the biopolymer and 68.01 GPa for the mineral area.

3. AFM-based nano-indentation – Oliver-Pharr method

An AFM system can also be used as a nanoindenter to investigate the mechanical properties of specimens. Figure S3 schematically represents a single cycle nano-indentation (load-unload curves). From these curves, we can extract mechanical properties as well as different energy scales like elastic or plastic energies. The elastic energy U_E is given by the area below the unloading curve and the plastic energy U_P corresponds to the difference in area between the loading and unloading curve (see Fig. S3). To determine the mechanical properties (hardness and elastic modulus) more steps are required and are discussed in the next section.

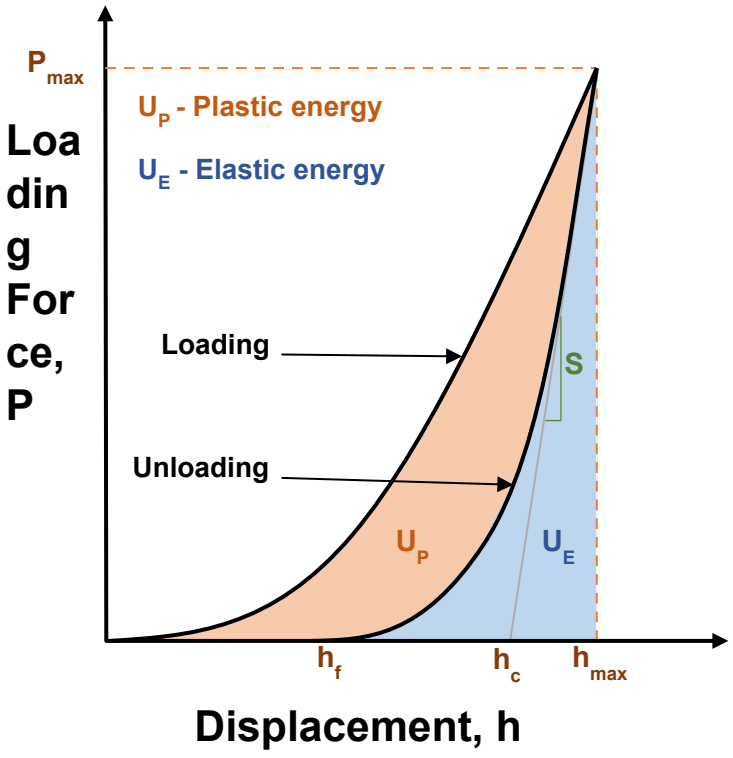

Figure S3. Schematic load-displacement curve. All parameters are explained and discussed in the text.

The most common method to determine the hardness and reduced modulus from an indentation cycle is Oliver-Pharr [13–15]. The loading force P is given by:

$$P = a(h - h_f)^m \tag{S7}$$

where h is the total indentation depth, h_f is the final displacement after completing the unloading process, a and m are the fitting parameters associated with the indenter shape.

The hardness (H) can be determined as the ratio of the maximum loading force (P_{max}) and the contact area between the indenter tip and the specimen at the maximum load (A):

$$H = \frac{P_{\max}}{A} \tag{S8}$$

The contact area A can be calculated as:

$$A = 24.5h_c^2 \tag{S9}$$

where h_c is the contact indentation depth determined from load-displacement curves

The reduced modulus (E_r) is the combined modulus of the indenter tip and the specimen and is determined from the relationship

$$E_r = \frac{S}{2}\frac{\sqrt{\pi}}{\sqrt{A}} \tag{S10}$$

where S is the initial unloading stiffness determined by the slope of the unloading curve dP/dh at the maximum load (see Fig. S3). Then the elastic modulus of the sample can be determined by the Hertzian model using equation S6.

Figure S4(a) represents the topography of a fused silica sample (Bruker, USA) after a nano-indentation cycle with 30 μN. All of the nano-indentations are done in a Smart SPM 1000 system (AIST-NT, USA) using a single crystal diamond NM-RC-C probe (Bruker, USA) with elastic modulus and Poisson's ratio of 1164 GPa and 0.0791, respectively[16]. The cross-sectional profiles of the indentation in Fig. S4(b) show the indented depth and width of 8.45 nm and 156 nm, respectively. The elastic modulus E is characterised by fitting the unloading curves in Fig. S4(c) using the Oliver-Pharr and Hertzian model, resulting in a value of 70.64 GPa. This is

again very similar to the manufacturer values of fused silica and shows the validity of our AFM-based nano-indentation measurements.

Due to the software of the AFM system, we had to perform load-unload curves without a hold period. Such a hold period can be important to reduce the impact of further creep after the maximal load on the unloading curve[17]. This can lead to negative slopes ('nose' shape) in the unload curve and thus wrong slope values that are important for the elastic modulus calculations. We have checked all indentation measurements and have not found any significant negative slopes in the unloading curves (also see Fig. S4 and Fig. S5). This could come from the fact that there is less creep in our experiments due to a lower maximum load in the AFM-based nano-indentation in comparison to standard indenter measurements. Due to the accuracy of our reference measurements on silica, we assume that our measurements are only slightly impacted by creep and the determination of the slope gives adequate values.

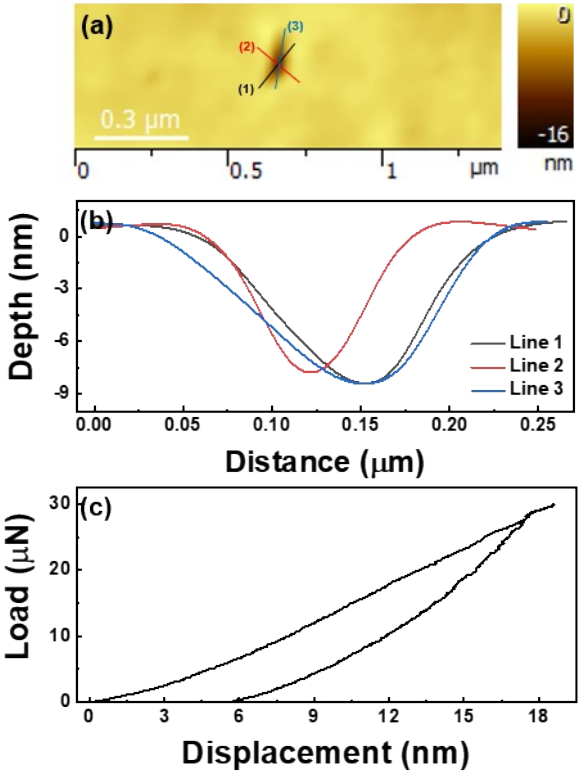

Figure S4. (a) Topography, (b) cross-sectional profiles along the black, red, and blue lines corresponding to the image (a); (c) Load-displacement curves of the nano-indentation on commercial fused-silica (Bruker) with the loading force at 30 µN.

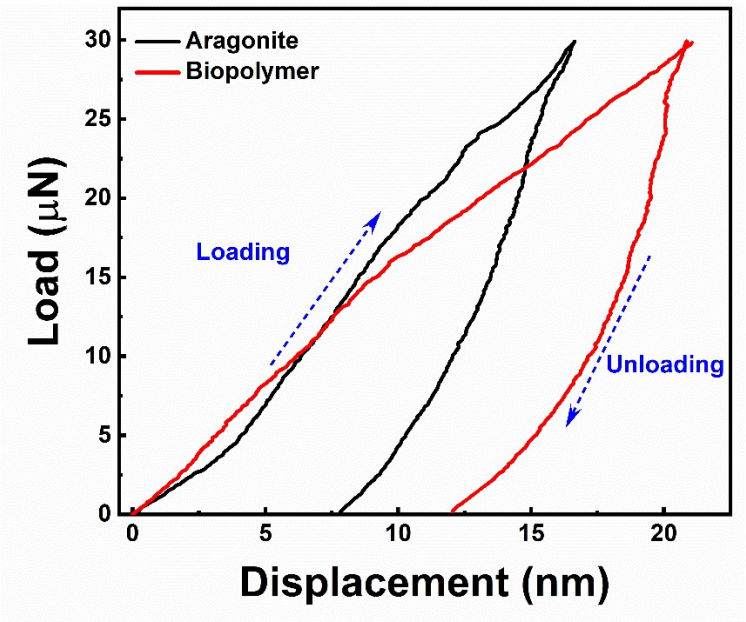

Figure S5. Load-displacement curves of aragonite and biopolymer regions at the same loading force of 30 μN.

Figure S5 shows examples of nano-indentation load-displacement curves on aragonite and biopolymer regions. The extracted values from the unloading curves and the calculated mechanical properties of Fig. S5 are shown in Table S2. These values provide a good example for the biopolymer and aragonite regions, however, all values mentioned in the main manuscript are average values over ten indentations for each area. Even though the maximum load in the aragonite and biopolymer area with 30 μN is the same, different maximum displacements h_{max} with 16.59 nm and 20.98 nm occur. This leads to a smaller contact area for the aragonite compared to the biopolymer regions and thus to higher hardness and elastic modulus in this area. The jump-like feature that can be seen at the maximum load in the biopolymer curve in Fig. S5 appears in roughly 1/3 of our measurements. It is a result of a maximum change in tip displacement by 3 Å. AFM-based nano-indentation measurements are less stable and more prone to noise, which can lead to small changes in height and rougher indentation curves. Thus, we assume this artifact to be a result of the stability of our system, which should not impact the accuracy of our measurements due to the small change in displacement.

Table S2. Data fitted to the nano-indentation unloading curves of aragonite and biopolymer in Fig. S5 using the Oliver-Pharr method

Parameters	**Aragonite**	**Biopolymer**
Slope S	3198	2374
Load P_{max} (μN)	30	30
Area A (μm^2)	1.66×10^{-3}	3.79×10^{-3}
Hardness H (GPa)	1.81	0.79
Reduced modulus E_r (GPa)	69.62	34.16
Elastic modulus E (GPa)	72.12	29.56
Elastic energy U_E (nJ)	1.86×10^{-4}	9.25×10^{-5}
Plastic energy U_P (nJ)	1.29×10^{-4}	3.72×10^{-4}

References

1 D. C. Hurley, in *Applied Scanning Probe Methods XI*, Springer Berlin Heidelberg, Berlin, Heidelberg, 2009, pp. 97–138.

2 D. C. Hurley and J. A. Turner, *J. Appl. Phys.*, 2007, **102**, 033509.

3 D. C. Hurley, M. Kopycinska-Müller, A. B. Kos and R. H. Geiss, *Meas. Sci. Technol.*, 2005, **16**, 2167–2172.

4 X. Zhou, H. Miao and F. Li, *Nanoscale*, 2013, **5**, 11885–11893.

5 A. Lakhtakia and R. J. Martín-Palma, *Engineered Biomimicry*, Elsevier, 2013.

6 Oxford Instruments, https://afmprobes.asylumresearch.com/ac160tsa-r3.html.

7 F. Barthelat, C.-M. Li, C. Comi and H. D. Espinosa, *J. Mater. Res.*, 2006, **21**, 1977–1986.

8 D. C. Lin, E. K. Dimitriadis and F. Horkay, *J. Biomech. Eng.*, 2007, **129**, 430–440.

9 S. L. Crick and F. C. P. Yin, *Biomech. Model. Mechanobiol.*, 2007, **6**, 199–210.

10 N. Gavara, *Sci. Rep.*, 2016, **6**, 1–13.

11 Asylum Research, *Applications Guide*, 2018.

12 Bruker, Fused silica, https://www.brukerafmprobes.com/p-3740-fsilica.aspx.

13 W. C. Oliver and G. M. Pharr, *J. Mater. Res.*, 2004, **19**, 3–20.

14 C. M. Smith, D. Jiang, J. Gong and L. Yin, *Mater. Chem. Phys.*, 2014, **148**, 1036–1044.

15 D. J. Shuman, A. L. M. Costa and M. S. Andrade, *Mater. Charact.*, 2007, **58**, 380–389.

16 C. A. Klein, *Mater. Res. Bull.*, 1992, **27**, 1407–1414.

17 B. J. Briscoe, L. Fiori and E. Pelillo, *J. Phys. D. Appl. Phys.*, 1998, **31**, 2395–2405.